nature neuroscience

Subtype-specific plasticity of inhibitory circuits in motor cortex during motor learning

Simon X Chen[1–3], An Na Kim[1–3], Andrew J Peters[1–3] & Takaki Komiyama[1–4]

Motor skill learning induces long-lasting reorganization of dendritic spines, principal sites of excitatory synapses, in the motor cortex. However, mechanisms that regulate these excitatory synaptic changes remain poorly understood. Here, using *in vivo* two-photon imaging in awake mice, we found that learning-induced spine reorganization of layer (L) 2/3 excitatory neurons occurs in the distal branches of their apical dendrites in L1 but not in the perisomatic dendrites. This compartment-specific spine reorganization coincided with subtype-specific plasticity of local inhibitory circuits. Somatostatin-expressing inhibitory neurons (SOM-INs), which mainly inhibit distal dendrites of excitatory neurons, showed a decrease in axonal boutons immediately after the training began, whereas parvalbumin-expressing inhibitory neurons (PV-INs), which mainly inhibit perisomatic regions of excitatory neurons, exhibited a gradual increase in axonal boutons during training. Optogenetic enhancement and suppression of SOM-IN activity during training destabilized and hyperstabilized spines, respectively, and both manipulations impaired the learning of stereotyped movements. Our results identify SOM inhibition of distal dendrites as a key regulator of learning-related changes in excitatory synapses and the acquisition of motor skills.

Motor skill learning involves changes in the motor cortex observed at several levels[1–9]. At the structural level, motor learning has been shown to induce reorganization of dendritic spines in the motor cortex, and the survival of learning-induced nascent spines is thought to be a basis for long-lasting motor memories[10,11]. However, little is known about the mechanisms that regulate the spatiotemporal specificity of these changes of excitatory synapses during motor learning. How does the circuit know when and where to modify synapses to encode a new motor skill? It is known that the excitability of dendrites is critical to controlling the plasticity of excitatory circuits, raising an intriguing possibility that local inhibitory neurons are involved in regulating the specificity of learning-related changes in synaptic circuits during motor learning.

Cortical GABAergic inhibitory neurons display a great diversity based on differences in their morphology, anatomical connectivity, electrophysiological properties and gene expression[12]. Different subtypes of inhibitory neurons target different domains of excitatory neurons, affording them the ability to control the spatiotemporal activity of excitatory neurons. For example, somatostatin-expressing inhibitory neurons (SOM-INs) typically project their axons to the uppermost layer of cortex, L1, where they inhibit distal portions of apical dendrites of excitatory neurons. In contrast, parvalbumin-expressing inhibitory neurons (PV-INs) mainly target and inhibit somatic and perisomatic regions of excitatory neurons and regulate their spike output. There is accumulating evidence that inhibition is important in controlling the plasticity of excitatory circuits[13–20]. However, contributions of distinct subtypes of inhibitory neurons in adult learning are just beginning to be understood.

In this study, we used *in vivo* two-photon imaging in awake mice to chronically monitor the dynamics of dendritic spines of excitatory neurons and axonal boutons of SOM-INs and PV-INs throughout motor learning. Chronic imaging of dendritic spines in the distal branches of apical dendrites and the perisomatic dendrites of L2/3 excitatory neurons revealed dendritic compartment–specific reorganization of dendritic spines. Imaging the same axonal branches of SOM-INs or PV-INs throughout learning, we found that motor learning induced subtype-specific plasticity of inhibitory circuits in the motor cortex. Manipulation of SOM-IN activity affected the stability of dendritic spines and blocked the formation of stereotyped movements. Our results uncover an important role of inhibitory neuron subtypes in regulating the spatiotemporal specificity of learning-related excitatory circuit plasticity.

RESULTS

Dendritic compartment-specific spine reorganization during motor learning

We adapted a cued lever-press task that we recently developed for mice to perform under a two-photon microscope[1]. In this task, mice under head fixation learn to use their left forelimb to press a lever beyond a set threshold during an auditory cue to receive a water reward (**Fig. 1a**). Mice showed a gradual improvement in performance with training over 11 sessions, one session per day (**Fig. 1b**), and the time from cue onset to achieving the reward significantly decreased over time (**Fig. 1c**). Furthermore, their lever-press movements became more reproducible (**Fig. 1d**), as shown by higher correlations of individual movements within and across later sessions (**Fig. 1e**). We recently showed that the motor cortex is required for the learning of

[1]Neurobiology Section, University of California, San Diego, La Jolla, California, USA. [2]Center for Neural Circuits and Behavior, University of California, San Diego, La Jolla, California, USA. [3]Department of Neurosciences, University of California, San Diego, La Jolla, California, USA. [4]Japan Science and Technology Agency, PRESTO, University of California, San Diego, La Jolla, California, USA. Correspondence should be addressed to T.K. (tkomiyama@ucsd.edu).

Received 24 March; accepted 28 May; published online 22 June 2015; doi:10.1038/nn.4049

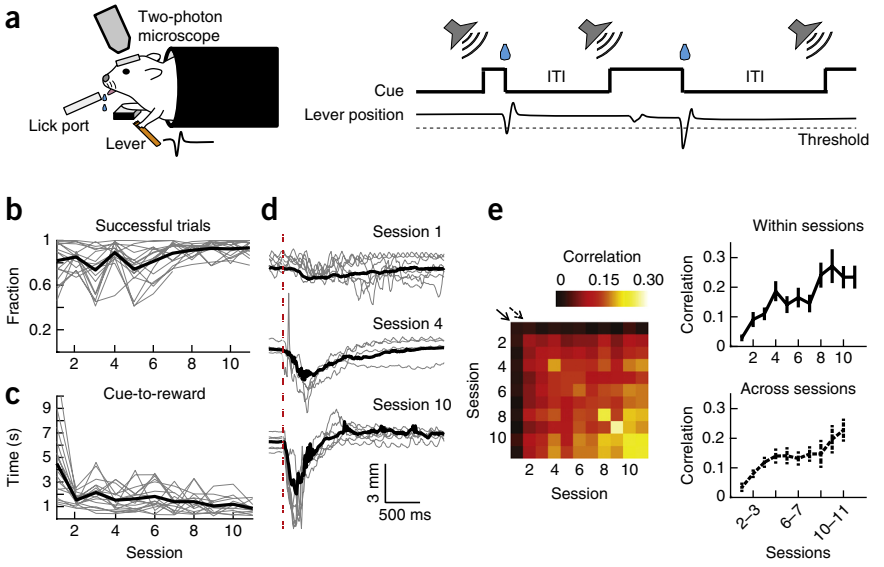

Figure 1 Lever-press task for head-fixed mice. (**a**) Schematic of experimental setup and task. ITI, intertrial interval. (**b**) Fraction of successful trials improves with learning ($P < 0.001$, one-way ANOVA, $n = 17$ mice). Gray, individual animals; black, mean. (**c**) Time from cue onset to reward decreases with learning ($P < 0.001$, one-way ANOVA). Gray, medians of individual animals; black, mean. (**d**) Example lever movement traces from one animal aligned by movement onset, showing the emergence of movement stereotypy with learning. Gray, ten individual trials; black, median of all trials; red dashed line, movement onset. (**e**), Left, trial-to-trial correlation of movement kinematics during learning. Each square represents the median value of the pairwise correlations of the rewarded movement traces of all trial pairs within the session pair, averaged across animals. Right, movement correlation (movement stereotypy) increases within and across sessions, corresponding to the diagonals shown by the solid and dashed arrows in the correlogram on the left (within sessions, $P < 0.001$; across sessions, $P < 0.001$, one-way ANOVA, $n = 17$ mice). Error bars indicate s.e.m.

stereotyped lever-press movements and that, during learning, L2/3 excitatory neurons in the motor cortex acquire an activity pattern that is reproducible from trial to trial[1]. This led us to examine the synaptic changes in the motor cortex during this learning.

To monitor the dynamics of excitatory synapses in the motor cortex, we labeled a sparse set of L2/3 neurons by injecting a mixture of adeno-associated viral (AAV) vectors encoding Cre recombinase and Cre-dependent GFP in the forelimb area of the right motor cortex of wild-type mice and applied chronic two-photon imaging in awake, head-fixed mice in every training session (**Fig. 2**). Daily imaging of the same dendritic branches on L2/3 excitatory neurons revealed specific changes in dendritic spines during learning (**Fig. 2b** and **Supplementary Fig. 1a,b**). In the distal branches of apical dendrites located in L1, spine formation was significantly increased during the

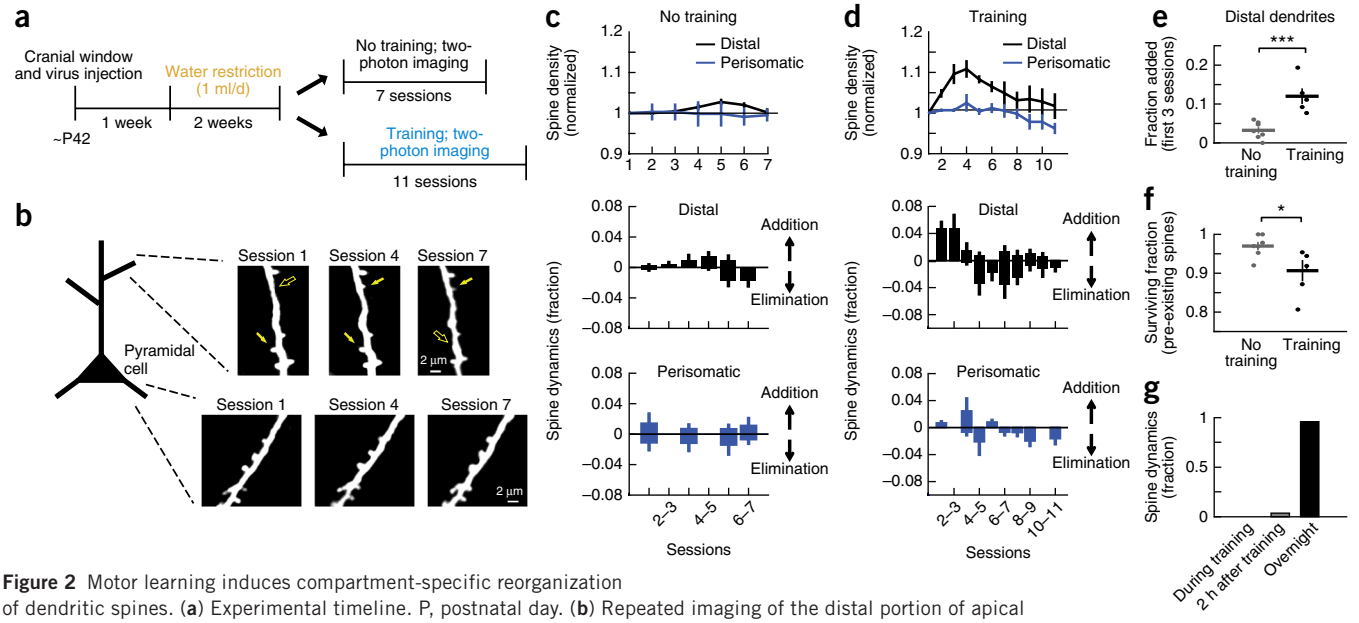

Figure 2 Motor learning induces compartment-specific reorganization of dendritic spines. (**a**) Experimental timeline. P, postnatal day. (**b**) Repeated imaging of the distal portion of apical dendrites (L1, 0–50 µm from pia) and perisomatic dendrites (L2/3, 150–200 µm) of L2/3 pyramidal cells throughout learning. Filled and open arrows indicate present and absent dynamic spines (that is, the spines that were added or eliminated during the course of training), respectively. (**c**) Mean spine density normalized to the initial session (top) and daily spine dynamics (bottom) of distal dendrites ($n = 7$ mice, 269 spines) and perisomatic dendrites ($n = 4$ mice, 120 spines) in no-training animals. (**d**) Mean spine density normalized to the initial session (top) and daily spine dynamics (bottom) of distal dendrites ($n = 5$ mice, 251 spines) and perisomatic dendrites ($n = 5$ mice, 206 spines) in training animals. Learning transiently increases spine density in distal but not perisomatic dendrites of L2/3 pyramidal cells (distal: $P < 0.001$ compared to no training; perisomatic: $P = 0.246$ compared to no training; two-way ANOVA). (**e**) Learning increases the spine addition rate in distal dendrites during the first three sessions. (**f**) Learning increases the elimination rate of pre-existing spines in the distal dendrites (fraction of pre-existing spines that remained until session 7). $^*P < 0.05$, $^{***}P < 0.001$; one-tailed bootstrap test. (**g**) Spine formation and elimination in the distal dendrites rarely occurred during (0%, 0 of 25) or within 2 h of (4%, 1 of 25) training sessions ($n = 3$ mice, 134 spines total). Error bars indicate s.e.m.

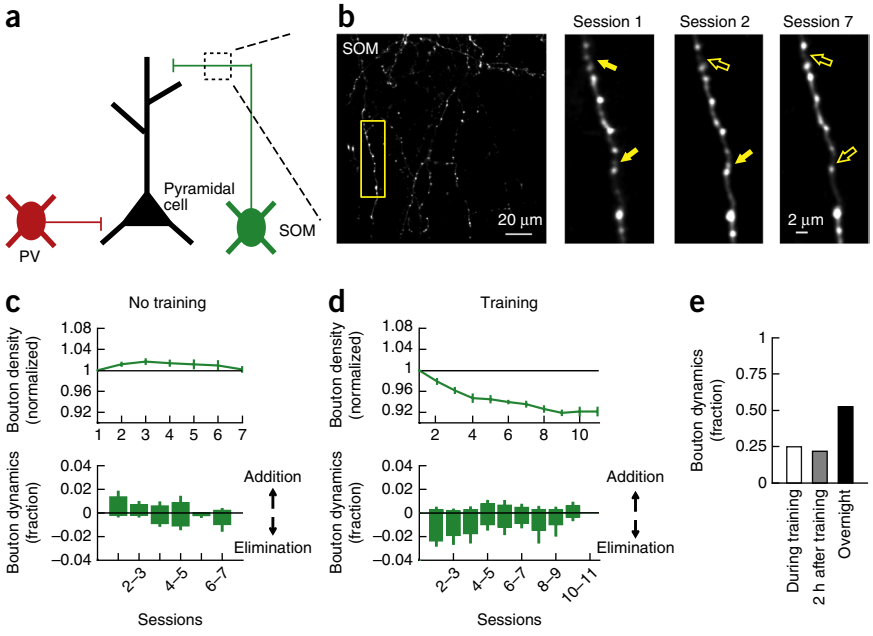

Figure 3 SOM-IN axonal boutons are rapidly eliminated following training. (**a**) SOM-INs mainly inhibit distal dendrites of excitatory neurons. (**b**) Left, a field of SOM-IN axons in L1 imaged throughout learning *in vivo*. Right, zoom of outlined area on the left. Filled and open arrows indicate present and absent dynamic boutons, respectively. (**c**) Mean normalized bouton density (top) and daily bouton dynamics (bottom) of SOM-INs in no-training animals ($n = 6$ mice, 464 boutons). (**d**) Mean normalized bouton density (top) and daily bouton dynamics (bottom) of SOM-INs in training animals ($n = 5$ mice, 433 boutons). SOM boutons decreased with training ($P < 0.001$, two-way ANOVA with *post hoc* Tukey's test, compared to no training) owing to an increase in bouton elimination ($P < 0.001$, one-tailed bootstrap). (**e**) Many bouton formation and elimination events for SOM-INs occurred during (25%, 8 of 32) and within 2 h of (22%, 7 of 32) training sessions ($n = 3$ mice, 258 boutons). Error bars indicate s.e.m.

first three sessions of training compared to that in untrained controls (**Fig. 2c–e**), followed by an increased elimination of spines that existed at the beginning of training ('pre-existing spines'; **Fig. 2f**). 75% (18 out of 24) of the spines that formed in the first three sessions of training were stable and remained until the end of the experiment. In contrast to the reorganization of distal spines, spines on perisomatic dendrites (<75 µm from soma) in L2/3 were relatively stable during learning (**Fig. 2c,d**). Spines on distal dendrites in the hindlimb area of the motor cortex were also stable during learning (**Supplementary Fig. 2**). These results establish that the learning of the lever-press task induces an area-specific and subcellular compartment–specific reorganization of excitatory synapses in the motor cortex.

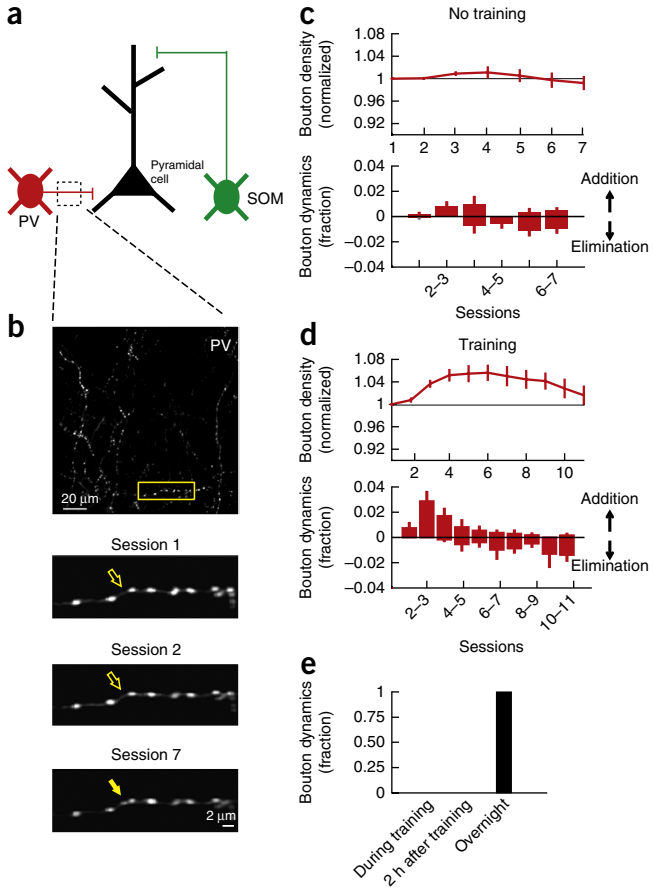

Subtype-specific plasticity of inhibitory circuits during motor learning

These observations suggest the existence of a mechanism that regulates the compartment specificity of spine plasticity. Since a growing body of evidence suggests that inhibitory circuits are important to the regulation of local excitatory synaptic plasticity[13–20], we asked whether motor learning induces plasticity of inhibitory circuits, focusing on SOM-INs and PV-INs because of their compartment-specific targeting. SOM-INs mainly inhibit distal dendrites of excitatory neurons while PV-INs mainly inhibit perisomatic regions (**Fig. 3a**)[12], and SOM- and PV-INs together comprise about two-thirds of cortical inhibitory neurons[21,22]. To monitor the dynamics of inhibitory synapses made by SOM- and PV-INs, we injected AAV encoding Cre-dependent GFP into the forelimb area of the right motor cortex of *SOM-Cre*[23] or *PV-Cre*[24] transgenic mice (**Supplementary Fig. 3**). In the GFP-labeled axons, boutons that presumably corresponded to presynaptic terminals[25] were clearly identifiable, and we could reliably follow the same axonal branches throughout learning. We imaged SOM-IN axons in L1, where they inhibit distal dendrites of excitatory neurons, repeatedly throughout 11 d of learning (**Fig. 3**). We found

Figure 4 PV-IN axonal boutons transiently increase during learning. (**a**) PV-INs mainly inhibit perisomatic regions. (**b**) Top, a field of PV-IN axons in L2/3. Bottom, zoom of outlined area above. (**c**) Mean normalized bouton density (top) and daily bouton dynamics (bottom) of PV-INs in no-training animals ($n = 6$ mice, 488 boutons). (**d**) Mean normalized bouton density (top) and daily bouton dynamics (bottom) of PV-INs in training animals ($n = 5$ mice, 396 boutons). PV boutons increase with training ($P < 0.001$, two-way ANOVA with *post hoc* Tukey's test, compared to no training). (**e**) All bouton formation and elimination events of PV-INs occurred overnight ($n = 3$ mice, 12 dynamic boutons out of 215 total boutons). Error bars indicate s.e.m.

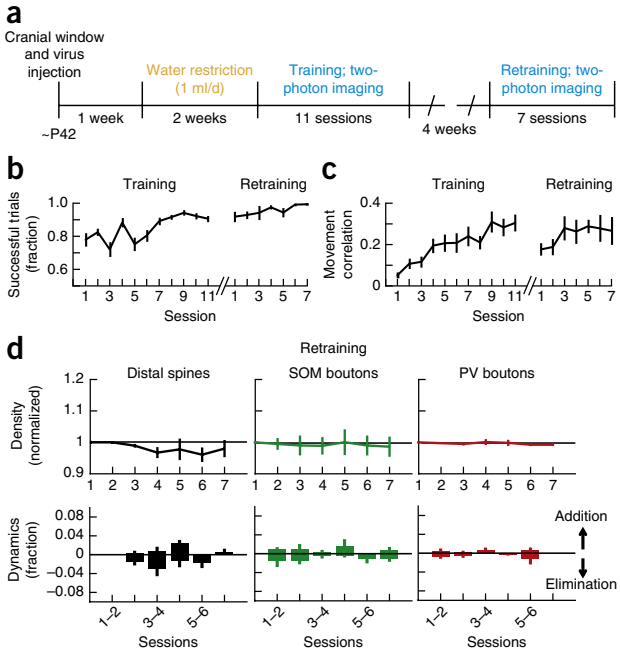

Figure 5 Synaptic reorganization is not observed during performance of a previously learned task. (**a**) Experimental timeline for retraining animals. (**b**) Fraction of successful trials in training ($n = 17$ mice) and retraining mice ($n = 10$ mice). (**c**) Median pairwise correlation of rewarded movements in each session in training and retraining mice. (**d**) Mean normalized density of distal spines, SOM boutons and PV boutons (top) and their daily dynamics in each session (bottom) during retraining (spine: $n = 3$ mice, 181 spines; SOM: $n = 3$ mice, 196 boutons; PV: $n = 3$ mice, 254 boutons). The density of spines and boutons showed no significant changes (spine: $P = 0.63$; SOM boutons: $P = 0.99$; PV boutons: $P = 0.91$; one-way ANOVA). Error bars indicate s.e.m.

that motor learning led to a significant reduction in the density of SOM boutons (**Fig. 3d**). By contrast, bouton density was stable in the forelimb area of untrained mice and in the hindlimb area during training (**Fig. 3c** and **Supplementary Fig. 2**).

Next we imaged PV-IN axons in L2/3, where they inhibit perisomatic regions of excitatory neurons (**Fig. 4**). In contrast to SOM-IN bouton density, motor learning induced a transient increase in the PV-IN bouton density compared to that in untrained controls (**Fig. 4b–d**). Taken together, these results indicate that motor learning induces opposing changes in SOM- and PV-INs, with a reduction in the density of boutons made by distally-targeting SOM-INs and an increase in the density of boutons made by perisomatically-targeting PV-INs.

One of the hallmarks of motor learning is that, once a skill is learned, it can be maintained for a long period of time without further training. Indeed, mice trained with the lever-press task maintained the skill 1 month after the original training, as shown by high success rates and movement stereotypy (**Fig. 5a–c**). During this retraining, spines and SOM and PV boutons were stable (**Fig. 5d**), demonstrating that the reorganization of local synaptic circuits is specific to the initial acquisition of a new motor skill.

To further understand the temporal dynamics of distal spines and inhibitory boutons with higher resolution, we next performed imaging at three time points each day—before training, immediately after training, and 2 h after training—in the first four behavioral sessions. We found that the vast majority of spine changes occurred between 2 h after training and the next day (**Fig. 2g**), consistent with a recent study[26]. PV bouton changes also followed a similar trend (**Fig. 4e**). However, about 50% of the changes in SOM boutons occurred during or within 2 h after behavioral sessions (**Fig. 3e**), indicating that training induces a rapid elimination of SOM boutons.

The observations of spine reorganization in distal dendritic branches and rapid loss of SOM-IN boutons during the initial phase of motor learning led us to hypothesize that the resulting reduction in dendritic inhibition creates a condition that allows learning-related changes in dendritic spines. However, SOM-INs inhibit not only excitatory neurons but also other inhibitory neuron types[21], and therefore the reduction in SOM boutons does not necessitate a reduction in inhibitory synapses onto excitatory neuron dendrites. To address this issue, we expressed GFP-tagged Gephyrin, a postsynaptic scaffolding protein at inhibitory synapses, in L2/3 excitatory neurons using *in utero* electroporation (**Fig. 6a**). This allowed us to monitor the dynamics of inhibitory synapses[16,17] in awake and behaving mice during motor learning. By repeatedly imaging the same distal branches of apical dendrites in L1 (**Fig. 6b** and **Supplementary Fig. 1f**), we found

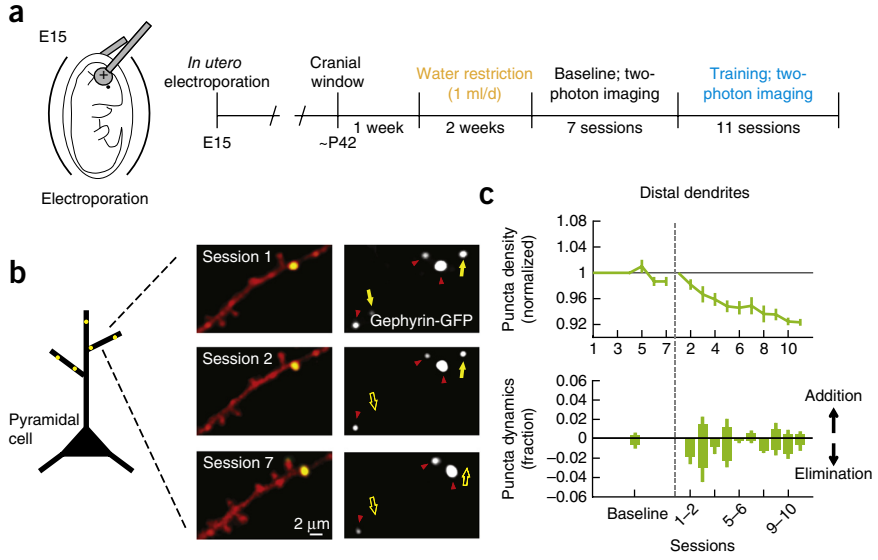

Figure 6 Elimination of inhibitory synapses in the distal dendrites of L2/3 pyramidal neurons during learning. (**a**) Schematic of *in utero* electroporation to express Gephyrin-GFP in neocortical L2/3 pyramidal neurons (left) and experimental timeline (right). E, embryonic day. (**b**) Left, representative images of a distal dendritic branch in red with Gephyrin-GFP puncta shown in green. Right, the Gephyrin-GFP channel only. Yellow filled and open arrows indicate present and absent dynamic puncta, respectively. Red arrowheads indicate stable puncta. (**c**) Mean normalized Gephyrin-GFP puncta density (top) and daily dynamics (bottom) during baseline (7 sessions, $n = 3$ mice, 138 puncta) and learning (11 sessions, $n = 4$ mice, 339 puncta). For baseline, punctum dynamics from all sessions are combined. Black dotted line represents the beginning of the behavioral training. Gephyrin-GFP puncta are reduced with training ($P < 0.001$, two-way ANOVA with *post hoc* Tukey's test, compared to baseline) owing to an increase in elimination of puncta compared to the baseline ($P < 0.001$, one-tailed bootstrap). Error bars indicate s.e.m.

that the density of GFP-positive puncta decreased during learning, compared to that in untrained controls (**Fig. 6c**). The time course and extent of Gephyrin-GFP dynamics mirrored those of SOM boutons. Thus, inhibitory synapses on distal dendrites of excitatory neurons are reduced during motor learning.

Manipulation of SOM-IN activity during learning affects spine stability

To test whether the reduced SOM inhibition during learning is essential for spine reorganization, we used optogenetics to activate SOM-INs during learning (**Fig. 7a**). We injected AAV encoding Cre-dependent channelrhodopsin-2 (ChR2) in *SOM-Cre; Thy1-GFP-S* double transgenic mice. In the Thy1-GFP-S line[27], a sparse set of cortical neurons are labeled, which allowed us to monitor dendritic spine dynamics without the use of Cre. We trained these mice and imaged the spines on distal dendrites in L1 daily as we mildly activated SOM-INs by delivering blue light (10-ms pulses at 3 Hz) through the imaging window during each training session (**Fig. 7b** and **Supplementary Fig. 1c**,**d**). This stimulation reliably evoked spiking of SOM-INs (**Supplementary Fig. 4a–c**), and repeated stimulation over days did not affect the survival of SOM-INs (**Supplementary Fig. 4d**,**e**). When ChR2 was activated in SOM-INs during training, a similar increase in spine formation rate was observed to that in control mice expressing tdTomato instead of ChR2 (sessions 1–3, **Fig. 7d**,**e**). However, SOM-IN activation prevented the stabilization of these learning-related nascent spines and also destabilized some of the pre-existing spines (**Fig. 7f**,**g**). As a result, the increase in spine density was abolished with SOM-IN activation (**Fig. 7c**). The spine dynamics were observed across multiple branches in both control and ChR2 animals (**Supplementary Fig. 5**). Neither ChR2 expression alone without blue light stimulation nor ChR2 stimulation without training affected spine dynamics (**Supplementary Fig. 6a**,**d**). These results suggest that the reduction in SOM-IN inhibition is an essential process regulating spine stabilization during learning.

If the reduction in SOM-IN inhibition is essential for learning-related spine reorganization, would SOM-IN inactivation during learning further enhance spine reorganization? To address this question, we next inactivated SOM-INs during learning by injecting AAV encoding Cre-dependent halorhodopsin (eNpHR3.0) in *SOM-Cre; Thy1-GFP-S* mice and delivering amber light (10-ms pulse at 10 Hz) in each training session. In this condition, learning-related spine formation occurred normally (**Fig. 7d**,**e** and **Supplementary Fig. 6d**) but spine elimination was almost completely abolished (**Fig. 7d**,**f**,**g**). This resulted in an increased spine density that was maintained until the end of training (**Fig. 7c**). Thus, spine dynamics is highly sensitive to the level of SOM inhibition.

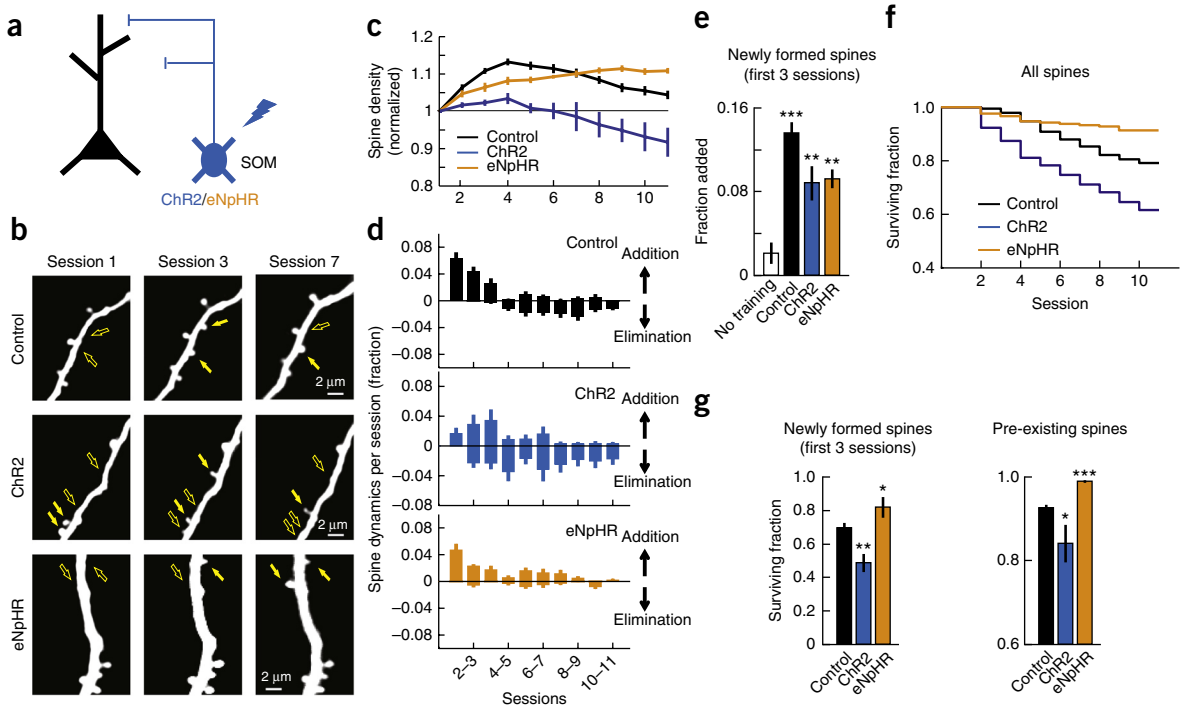

Figure 7 Manipulation of SOM-IN activity during training disrupts spine stability. (**a**) ChR2 or eNpHR was expressed to activate or inactivate SOM-INs, respectively, during training sessions. tdTomato was expressed in control animals. (**b**) Repeated imaging of L1 distal dendritic branches of excitatory neurons of control, ChR2 and eNpHR animals throughout learning. Filled and open arrows indicate present and absent dynamic spines, respectively. (**c**) Mean normalized spine density in control animals ($n = 12$ mice, 665 spines), animals in which SOM-INs were activated during training (ChR2; $n = 5$ mice, 255 spines) and animals in which SOM-INs were inactivated during training (eNpHR; $n = 6$ mice, 397 spines). SOM-IN activation blocked learning-related increase of spine density ($P < 0.001$, 2-way ANOVA with *post hoc* Tukey's test, compared to control), and SOM-IN inactivation extended the spine density increase ($P < 0.001$, two-way ANOVA with *post hoc* Tukey's test, compared to control). (**d**) Daily spine dynamics in control, ChR2 and eNpHR animals during training. (**e**) Training-induced spine formation in the first three sessions of control, ChR2 and eNpHR animals. $^{**}P < 0.01$, $^{***}P < 0.001$, one-tailed bootstrap with Bonferroni correction compared to no training. (**f**) Kaplan-Meier survival curves for all dendritic spines. Spines are less stable when SOM-INs are activated and more stable when SOM-INs are inactivated, compared to control ($P < 0.001$, log-rank test with Bonferroni correction). (**g**) Left, fraction of newly formed spines in the first three sessions of training that remained until the end of the training. SOM-IN activation reduced the stability of learning-related new spines whereas SOM-IN inactivation hyperstabilized them. Right, fraction of pre-existing spines that remained until the end of training. $^{*}P < 0.05$, $^{**}P < 0.01$, $^{***}P < 0.001$, one-tailed bootstrap test with Bonferroni correction compared to control. Error bars indicate s.e.m.

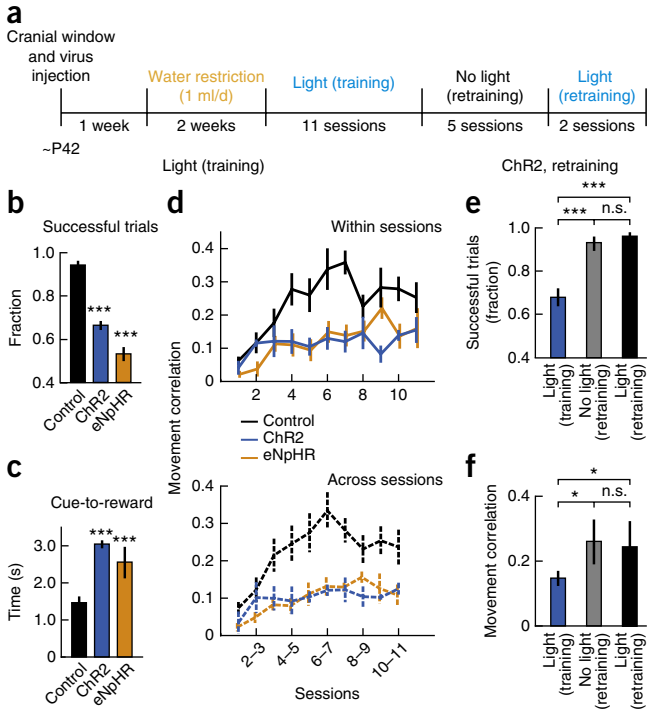

Figure 8 Manipulation of SOM-IN activity impaired the formation of stereotyped movements. (**a**) Experimental timeline. (**b**) Mean fractions of successful trials in sessions 7–11. Control animals achieved a reward in a larger fraction of trials than ChR2 or eNpHR animals. $***P < 0.001$, one-tailed bootstrap test with Bonferroni correction, compared to control. (**c**) Time from cue onset to achieve reward is longer in ChR2 and eNpHR animals compared to control. $***P < 0.001$, one-tailed bootstrap test with Bonferroni correction compared to control. (**d**) Medians of trial-to-trial movement correlations. Values are lower in ChR2 and eNpHR animals, indicating their failure to form stereotyped movement patterns (within sessions: $P < 0.001$; across sessions: $P < 0.001$; compared to control, two-way ANOVA with *post hoc* Tukey's test). (**e**) Mean fractions of successful trials of ChR2 animals in the last two sessions of training with light, retraining without light, and retraining with light ($n = 5$ mice). (**f**) Mean correlation of movements within sessions in all three conditions. Once the animals acquired the motor skill, SOM-IN stimulation did not affect the performance ($P > 0.1$, retraining with no light versus retraining with light). $*P < 0.05$, $***P < 0.001$, one-tailed bootstrap test with Bonferroni correction; n.s., not significant. Error bars indicate s.e.m.

Manipulation of SOM-IN activity impairs learning

If proper spine reorganization is important for learning, it would be predicted that manipulations that changed spine dynamics will also affect learning. Indeed, mice that had SOM-INs activated during training missed more trials than control mice (**Fig. 8b**) and took a significantly longer time to achieve the threshold for a reward from the cue onset (**Fig. 8c**). Furthermore, activation of SOM-INs blocked the formation of stereotyped movements, as shown by the low trial-to-trial correlation of their movement kinematics throughout training (**Fig. 8d**). Similarly, SOM-IN inactivation also impaired motor learning, as shown by a lower fraction of successful trials, longer time to achieve a reward and lower correlation of movement kinematics (**Fig. 8b–d**). ChR2 expression alone without blue light stimulation had no effect on spine dynamics and learning (**Supplementary Fig. 6e**).

The observed effects of SOM-IN manipulation on spine dynamics and learning were in stark contrast to when PV-INs were activated using the same protocol, which affected neither spine dynamics nor behavior (**Supplementary Fig. 6b,d,e**), indicating that the impairment of learning-related spine dynamics and motor learning was specific to SOM-IN activation. In addition, after the initial experiments, we trained the same SOM-IN ChR2 mice without blue light delivery, which led them to reach expertise similar to that of control mice (**Fig. 8a,e,f**). Notably, once the mice had acquired the skill, SOM-IN activation did not affect their performance (**Fig. 8e,f**). Thus, the effect of SOM-IN activation is specific to the acquisition of a new motor skill. Together our results from SOM-IN activation and inactivation experiments suggest that the plasticity of SOM-INs during learning enables the appropriate level of SOM-IN inhibition that is essential for the learning-related spine stabilization and elimination. They are also consistent with the notion that the stabilization of learning-related spines and elimination of some of the other, presumably unnecessary spines, ensured by an appropriate level of SOM inhibition, are indeed necessary for motor learning.

DISCUSSION

Previous studies showed that various sensory experience and learning paradigms cause a rearrangement of local synapses[28–30]. In particular, motor learning induces the establishment of new spines in the motor cortex[1,10,31], which correlates with long-lasting motor memories[11]. Here we extend these studies by investigating spine plasticity in different dendritic compartments, as well as bouton plasticity of two genetically defined inhibitory neuron types, in the motor cortex during motor learning. We found that learning-related spine plasticity occurred in L1 distal dendritic branches but not in perisomatic regions of L2/3 excitatory neurons. Coinciding with this compartment-specific spine reorganization was subtype-specific plasticity of inhibitory circuits, in which distally-targeting SOM-INs decreased their synapses in L1 and perisomatically-targeting PV-INs increased their synapses. Our results provide evidence for a mechanism by which subtype-specific inhibitory circuit plasticity regulates the spatiotemporal specificity of learning-related structural plasticity of excitatory synapses and thus the acquisition of motor skills.

Inhibitory control of excitatory circuit plasticity

We show that learning-related spine reorganization is restricted to the dendritic compartment that is inhibited by SOM-INs and that the number of SOM-IN boutons rapidly decreases during the initial phase of learning. Importantly, previous studies have implicated the involvement of NMDA receptor–dependent LTP-like mechanisms in long-term stabilization of nascent dendritic spines *in vitro*[32] and in motor learning *in vivo*[33]. Furthermore, the level of GABAergic inhibition can control dendritic excitability and synaptic plasticity, with more and less inhibition favoring synaptic depression and potentiation, respectively[34–36]. Recent *in vivo* imaging studies showed that dendritic calcium events can predict the plasticity of response properties of hippocampal neurons[37] and the synaptic plasticity in the motor cortex[38]. The latter study also showed that the branch specificity of dendritic calcium events is controlled by local inhibition. In light of these previous studies, we postulate that the reduced inhibition of distal dendrites by SOM-INs that we identify here during learning makes the local dendrites more depolarized, creating a condition that favors synaptic potentiation and the stabilization of learning-related spines.

The notion that subtype-specific inhibitory circuit plasticity regulates compartment-specific spine plasticity is an extension of previous studies showing inhibitory gating of excitatory plasticity[13–20]. For example, a study demonstrated that monocular deprivation induces dendritic branch retractions in L2/3 inhibitory neurons and a loss of inhibitory inputs onto neighboring pyramidal cells in the visual

cortex of adult mice. It has been proposed that the reduced inhibitory inputs enable excitatory plasticity to strengthen the inputs from the non-deprived eye[20]. Our observations of the rapid loss of SOM-IN boutons and the bidirectional effects of SOM-IN inhibition on spine stability in the optogenetic manipulations further demonstrate that spine stability on distal dendrites is exquisitely sensitive to the level of SOM-IN inhibition: too much or too little SOM inhibition is detrimental to spine reorganization and motor learning. Manipulation of the activity of inhibitory neurons could in theory nonspecifically affect circuit activity and plasticity. However, two lines of evidence argue against this possibility. First, SOM-IN activation after learning did not affect learned behavior (**Fig. 8e**,**f**). Second, activation of PV-INs during learning with the same protocol did not affect spine dynamics or learning (**Supplementary Fig. 6**). While we cannot claim that SOM-INs are the only circuit component whose manipulation affects spine dynamics and learning, these results support a unique role of SOM-INs in regulating learning-related plasticity in distal dendritic branches.

Contrary to SOM-IN boutons, we observed a transient increase in PV-IN boutons during learning. PV-INs control the spike output of excitatory neurons by inhibiting their perisomatic regions, which are the regions we find to be relatively stable during motor learning. We speculate that this increase of PV-IN boutons is a homeostatic response to the learning-related reduction of SOM-IN inhibition and the resulting increase in the excitability of excitatory neurons. Indeed, homeostatic changes in inhibition have been found in PV-INs but not in SOM-INs[39]. Together our results underscore the importance of intricate interactions between excitation and inhibition in learning-related circuit plasticity.

METHODS

Methods and any associated references are available in the online version of the paper.

Note: Any Supplementary Information and Source Data files are available in the online version of the paper.

ACKNOWLEDGMENTS

We thank C. Levelt (Netherlands Institute for Neuroscience) for the Gephyrin-GFP construct and B. Bloodgood, R. Malinow and members of the Komiyama laboratory for comments and discussions. This work was supported by grants from Japan Science and Technology Agency (PRESTO), Pew Charitable Trusts, Alfred P. Sloan Foundation, David & Lucile Packard Foundation, Human Frontier Science Program, McKnight Foundation, US National Institutes of Health (R01 NS091010A), University of California San Diego Center for Brain Activity Mapping and New York Stem Cell Foundation (NYSCF) to T.K. S.X.C. is a Human Frontier Science Program postdoctoral fellow. A.J.P. is supported by the Neuroplasticity of Aging Training Grant (AG000216). T.K. is a NYSCF-Robertson Investigator.

AUTHOR CONTRIBUTIONS

S.X.C. and T.K. conceived the project. A.J.P. and T.K. developed the task. A.N.K. performed the PV-IN experiments. A.J.P. performed the *in vivo* cell-attached recordings. All other experiments were performed by S.X.C. with assistance by A.N.K. S.X.C. and T.K. analyzed the data with assistance from A.J.P. and wrote the manuscript with inputs from A.J.P. and A.N.K.

COMPETING FINANCIAL INTERESTS

The authors declare no competing financial interests.

1. Peters, A.J., Chen, S.X. & Komiyama, T. Emergence of reproducible spatiotemporal activity during motor learning. *Nature* **510**, 263–267 (2014).
2. Costa, R.M., Cohen, D. & Nicolelis, M.A. Differential corticostriatal plasticity during fast and slow motor skill learning in mice. *Curr. Biol.* **14**, 1124–1134 (2004).
3. Huber, D. *et al.* Multiple dynamic representations in the motor cortex during sensorimotor learning. *Nature* **484**, 473–478 (2012).
4. Nudo, R.J., Milliken, G.W., Jenkins, W.M. & Merzenich, M.M. Use-dependent alterations of movement representations in primary motor cortex of adult squirrel monkeys. *J. Neurosci.* **16**, 785–807 (1996).
5. Rioult-Pedotti, M.S., Friedman, D. & Donoghue, J.P. Learning-induced LTP in neocortex. *Science* **290**, 533–536 (2000).
6. Komiyama, T. *et al.* Learning-related fine-scale specificity imaged in motor cortex circuits of behaving mice. *Nature* **464**, 1182–1186 (2010).
7. Sanes, J.N. & Donoghue, J.P. Plasticity and primary motor cortex. *Annu. Rev. Neurosci.* **23**, 393–415 (2000).
8. Rokni, U., Richardson, A.G., Bizzi, E. & Seung, H.S. Motor learning with unstable neural representations. *Neuron* **54**, 653–666 (2007).
9. Picard, N., Matsuzaka, Y. & Strick, P.L. Extended practice of a motor skill is associated with reduced metabolic activity in M1. *Nat. Neurosci.* **16**, 1340–1347 (2013).
10. Xu, T. *et al.* Rapid formation and selective stabilization of synapses for enduring motor memories. *Nature* **462**, 915–919 (2009).
11. Yang, G., Pan, F. & Gan, W.B. Stably maintained dendritic spines are associated with lifelong memories. *Nature* **462**, 920–924 (2009).
12. Markram, H. *et al.* Interneurons of the neocortical inhibitory system. *Nat. Rev. Neurosci.* **5**, 793–807 (2004).
13. Hensch, T.K. Critical period plasticity in local cortical circuits. *Nat. Rev. Neurosci.* **6**, 877–888 (2005).
14. Levelt, C.N. & Hubener, M. Critical-period plasticity in the visual cortex. *Annu. Rev. Neurosci.* **35**, 309–330 (2012).
15. Froemke, R.C., Merzenich, M.M. & Schreiner, C.E. A synaptic memory trace for cortical receptive field plasticity. *Nature* **450**, 425–429 (2007).
16. Chen, J.L. *et al.* Clustered dynamics of inhibitory synapses and dendritic spines in the adult neocortex. *Neuron* **74**, 361–373 (2012).
17. van Versendaal, D. *et al.* Elimination of inhibitory synapses is a major component of adult ocular dominance plasticity. *Neuron* **74**, 374–383 (2012).
18. Donato, F., Rompani, S.B. & Caroni, P. Parvalbumin-expressing basket-cell network plasticity induced by experience regulates adult learning. *Nature* **504**, 272–276 (2013).
19. Kuhlman, S.J. *et al.* A disinhibitory microcircuit initiates critical-period plasticity in the visual cortex. *Nature* **501**, 543–546 (2013).
20. Chen, J.L. *et al.* Structural basis for the role of inhibition in facilitating adult brain plasticity. *Nat. Neurosci.* **14**, 587–594 (2011).
21. Pfeffer, C.K., Xue, M., He, M., Huang, Z.J. & Scanziani, M. Inhibition of inhibition in visual cortex: the logic of connections between molecularly distinct interneurons. *Nat. Neurosci.* **16**, 1068–1076 (2013).
22. Rudy, B., Fishell, G., Lee, S. & Hjerling-Leffler, J. Three groups of interneurons account for nearly 100% of neocortical GABAergic neurons. *Dev. Neurobiol.* **71**, 45–61 (2011).
23. Taniguchi, H. *et al.* A resource of Cre driver lines for genetic targeting of GABAergic neurons in cerebral cortex. *Neuron* **71**, 995–1013 (2011).
24. Hippenmeyer, S. *et al.* A developmental switch in the response of DRG neurons to ETS transcription factor signaling. *PLoS Biol.* **3**, e159 (2005).
25. De Paola, V. *et al.* Cell type-specific structural plasticity of axonal branches and boutons in the adult neocortex. *Neuron* **49**, 861–875 (2006).
26. Yang, G. *et al.* Sleep promotes branch-specific formation of dendritic spines after learning. *Science* **344**, 1173–1178 (2014).
27. Feng, G. *et al.* Imaging neuronal subsets in transgenic mice expressing multiple spectral variants of GFP. *Neuron* **28**, 41–51 (2000).
28. Holtmaat, A. & Svoboda, K. Experience-dependent structural synaptic plasticity in the mammalian brain. *Nat. Rev. Neurosci.* **10**, 647–658 (2009).
29. Kasai, H., Fukuda, M., Watanabe, S., Hayashi-Takagi, A. & Noguchi, J. Structural dynamics of dendritic spines in memory and cognition. *Trends Neurosci.* **33**, 121–129 (2010).
30. Caroni, P., Donato, F. & Muller, D. Structural plasticity upon learning: regulation and functions. *Nat. Rev. Neurosci.* **13**, 478–490 (2012).
31. Fu, M., Yu, X., Lu, J. & Zuo, Y. Repetitive motor learning induces coordinated formation of clustered dendritic spines *in vivo*. *Nature* **483**, 92–95 (2012).
32. Hill, T.C. & Zito, K. LTP-induced long-term stabilization of individual nascent dendritic spines. *J. Neurosci.* **33**, 678–686 (2013).
33. Hasan, M.T. *et al.* Role of motor cortex NMDA receptors in learning-dependent synaptic plasticity of behaving mice. *Nat. Commun.* **4**, 2258 (2013).
34. Hayama, T. *et al.* GABA promotes the competitive selection of dendritic spines by controlling local Ca2+ signaling. *Nat. Neurosci.* **16**, 1409–1416 (2013).
35. Gidon, A. & Segev, I. Principles governing the operation of synaptic inhibition in dendrites. *Neuron* **75**, 330–341 (2012).
36. Steele, P.M. & Mauk, M.D. Inhibitory control of LTP and LTD: stability of synapse strength. *J. Neurophysiol.* **81**, 1559–1566 (1999).
37. Sheffield, M.E. & Dombeck, D.A. Calcium transient prevalence across the dendritic arbour predicts place field properties. *Nature* **517**, 200–204 (2015).
38. Cichon, J. & Gan, W.B. Branch-specific dendritic Ca^{2+} spikes cause persistent synaptic plasticity. *Nature* **520**, 180–185 (2015).
39. Xue, M., Atallah, B.V. & Scanziani, M. Equalizing excitation-inhibition ratios across visual cortical neurons. *Nature* **511**, 596–600 (2014).

ONLINE METHODS

Animals. All procedures were in accordance with protocols approved by UCSD institutional Animal Care and Use Committee and guidelines of the US National Institutes of Health. Mice were acquired from Jackson Laboratories (PV-Cre (008069), SOM-Cre (013044), Thy1-EGFP (011070)) and Charles River Laboratory (C57BL/6 wild type). All animals before water restriction were group housed and all animals under water restriction were singly housed in disposable plastic cages with standard bedding in a room on a reversed light cycle (12 h/12 h). Experiments were typically performed during the dark period. All animals used for imaging experiments were water restricted, regardless of whether they were trained or not.

Surgery and virus injection. Surgical procedures were performed as previously described[1]. Adult mice (6 weeks or older, male and female) were anesthetized with isoflurane and injected with Baytril (10 mg/kg), dexamethasone (2 mg/kg) and buprenorphine (0.1 mg/kg) subcutaneously at the beginning to prevent infection, inflammation and discomfort. A custom head-plate was glued and cemented to the skull. Craniotomy (~3 mm) was performed over the right caudal forelimb area (300 μm anterior and 1,500 μm lateral from the bregma). For the hindlimb area, craniotomy was made at 1,500 μm posterior and 1,500 μm lateral from the bregma. All coordinates were based on previous microstimulation experiments[40–43]. Sparse labeling of L2/3 neurons was achieved by injecting viral solutions in the center of craniotomy at three locations (~500 μm apart), 20–30 nL at each site (~250 μm depth). For imaging distal branches of apical dendrites of L2/3 pyramidal cells, a mixture of AAV2/1-CAG-FLEX-GFP (1:1) and AAV2/1-CMV-PI-Cre (1:5,000) diluted in saline was injected into C57BL/6 wild-type mice. For imaging perisomatic dendrites of L2/3 pyramidal cells, a more dilute mixture (AAV2/1-CAG-FLEX-GFP (1:1) and AAV2/1-CMV-PI-Cre (1:15,000)) was used for sparser labeling. For L2/3 PV or SOM axonal bouton imaging, AAV2/1-CAG-FLEX-GFP (1:100) diluted in saline was injected into PV-Cre or SOM-Cre mice, respectively. All viruses were purchased from UPenn Vector Core. Following the virus injections, a glass window was implanted over the craniotomy. The edges between the window and the skull were filled with 1.5% agarose and the window was secured with dental acrylic.

***In utero* electroporation.** Surgical procedures were performed as previously described[44]. To target neocortical L2/3 neurons, timed-pregnant female C57BL/6 mice (E15) were anesthetized with isoflurane and injected with Baytril (10 mg/kg), dexamethasone (2 mg/kg) and buprenorphine (0.1 mg/kg) subcutaneously at the beginning to prevent infection, inflammation and discomfort. Embryos were injected with ~1–2 μL of a mixture of plasmid, Gephyrin-GFP (0.5 μg/μL, gift from C. Levelt) and tdTomato (2 μg/μL), into the left lateral ventricle. Five electric pulses (intensity = 40 V, duration = 50 m, frequency = 1 Hz) were delivered, targeting the motor cortex, using a square wave electroporator (Harvard Apparatus).

Immunohistochemistry. Coronal sections (50 μm) were cut with a microtome, blocked in 4% normal goat serum in PBS and incubated overnight at 4 °C with primary antibodies diluted in blocking solution. After washing, sections were incubated in Alexa Fluor–conjugated secondary antibodies for 2 h at room temperature, mounted and imaged (Zeiss Axio Imager). The primary and secondary antibodies and dilutions used were as follows: rabbit anti-PV (1:3000, Swant, PV27), rabbit anti-SOM (1:250, Immunostar, 20089), Alexa 350 goat anti-rabbit (1:200, Life Technologies, A21068).

Behavior. Two weeks after surgery, mice were water-restricted to 1 mL/d. After ~14 d of water restriction, mice were trained 1 session/d for 11 sessions under a two-photon microscope. The hardware and software used for behavioral training have been previously described[1]. Lever position was continuously monitored through a piezoelectric flexible force transducer. A 6-kHz tone marked the cue period (up to 30 s in the first session, up to 10 s in subsequent sessions) during which a successful lever-press was rewarded with water (~10 μL per trial) paired with a 500-ms, 12-kHz tone, followed by an intertrial interval (variable duration of 2–4 s in the first session and 5–10 s in subsequent sessions). A successful lever-press was defined as crossing of two thresholds (upper threshold ~0.5 mm; lower threshold ~1.5 mm in sessions 1 and 2, ~3.0 mm in sessions 3 and 4, and ~4.5 mm in sessions 5–11) within 200 ms. The upper threshold ensured that the animal did not hold the lever near the lower threshold. The lower lever thresholds were incrementally increased to encourage the learning of a novel movement. Failure to pass the thresholds during the cue period resulted in a loud white-noise sound and the start of an intertrial interval. Lever presses during the intertrial interval were neither rewarded nor punished. Each animal typically performed ~100–150 trials/d and received ~1 mL of water reward. Each training session was terminated when the animal reached 100 successful trials or when it stopped performing. Retraining was performed 4 weeks after the initial training. Mice were trained 1 session/d for 7 sessions using the final threshold (~4.5 mm).

Movement analysis. Voltage traces from the piezoelectric lever were parsed into movement and quiescent bouts and downsampled from 10 kHz to 1 kHz. Lever trajectories on different trials were compared from the onset of the rewarded movement to 2 s after the onset of movement. Similarity of lever trajectories across trials was computed by Pearson correlation. Rewarded movements that started before the onset of the cue stimulus were excluded from analysis. Movement bouts were identified as previously described[1]; in brief, movement was detected by a velocity threshold, and the onset and offset of movement bouts were refined by the position of the lever respectively leaving or entering a stable state.

Imaging and image processing. Imaging was performed in awake mice at the beginning of each training session and, in a subset of animals, also at the end of each training session and 2 h after the end of the training session. Images were acquired using a commercial two-photon microscope (B-Scope, Thorlabs) with a 16× objective (NIKON) with excitation at 925 nm (Ti-sapphire laser, Newport) at ~28 Hz, 20 frames per plane, 80–120 planes per animal with a 1-μm *z*-axis step size. For spine imaging, distal dendritic branches were located within 100 μm of the pial surface (L1) and perisomatic dendrites were between ~150 and 250 μm (L2/3). For axonal bouton imaging, axonal branches of SOM-INs and PV-INs were located within 100 μm (L1) and at ~150–250 μm (L2/3) from the pial surface, respectively. For Gephyrin-GFP puncta imaging, the baseline group was a subset of mice that were later used for training, but the images were taken on separate dendritic branches. All dendritic branches for imaging of Gephyrin-GFP puncta were located within 100 μm of the pial surface (L1). Images were acquired at a resolution of 512 × 512 pixels, encompassing ~94 × 85 μm (distal dendrites and Gephyrin-GFP), ~54 × 40 μm (perisomatic dendrites) and ~138 × 128 μm (boutons). Distal dendrites in 4 no-training mice were imaged at ~54 × 40 μm so that they could be scored blindly with the images of perisomatic dendrites. Lateral motion for each image plane (20 frames) was corrected by full-frame cross-correlation image alignment (Turboreg[45] plug-in in ImageJ), using the average of the 5 most consistent consecutive frames as the reference image. Following this lateral motion correction, all 20 frames in a plane were averaged, and different image planes were then aligned using recursive alignment of stacks of images using Stackreg (ImageJ). Represented images shown in figures are projections from 3D image stacks containing the dendritic or axonal segments of interest. The images were processed with linear smoothing and look-up-table adjustments for presentation using ImageJ.

Image analysis. Spine and axonal bouton dynamics were manually scored and tracked over the entire 11 sessions in three dimensions using a custom program in IGOR (J. Boyd and K. Haas, University of British Columbia). The program provides a platform for manual scoring by spatially aligning the image stacks in 3D. Dendritic spines, axonal boutons or Gephyrin puncta were then identified, measured and tracked in 3D stacks manually across all time points on the basis of the published criteria[17,25,46]. In all optogenetics experiments, the experimenter was blinded to the condition (opsin versus control) and the scorer was again blinded to the condition (opsin versus control), behavioral status of the animal (learned versus not learned versus not trained) and session numbers. For other experiments, the scorer was blinded to the session number of each image, which was randomized. This excludes the possibility of subjective bias favoring addition or elimination of spines, boutons or puncta. After the blind scoring, session numbers were revealed and scoring was corrected with the following criteria: if a spine, bouton or punctum was scored as absent in one session (session X) and present in the immediately preceding (session $X-1$) and following (session $X+1$) sessions, then it was called present on session X. Furthermore, if a spine was scored as present in one session (session X) and absent in the immediately preceding (session X − 1) and following (session $X+1$) sessions, then it was called

doi:10.1038/nn.4049

absent on session *X*. No more than one correction was applied on any given spine, bouton or punctum. If a spine, bouton or punctum contained these gaps after one correction, then it was excluded from following analyses. In total, 6.7% of spines, boutons or puncta were corrected (487 of 7,215) and only 0.6% were excluded (45 of 7,215). While this corrected for mistakes in scoring, we may be slightly underestimating the dynamics. The blind scoring results matched those from independent scoring of the same data set without shuffling (data not shown). The total density of spines, boutons and puncta scored in each session was normalized to the initial session. The number of mice, spine/bouton/punctum, branch number, branch length and density analyzed in all experimental conditions are summarized in **Supplementary Table 1**.

Optogenetic experiments. For ChR2 or eNpHR expression in SOM-INs, AAV2/1-CAG-FLEX-ChR2-tdTomato (UPenn Vector Core) or AAV2/1-CAG-FLEX-eNpHR3.0-mCherry (Neurophotonic Center, University of Laval), respectively, was injected at five sites (~500 μm apart), 100 nL at each site (~250 μm depth) in the right caudal forelimb area of SOM-Cre:Thy1-EGFP mice. For ChR2 expression in PV-INs, AAV2/1-CAG-FLEX-ChR2-tdTomato was injected at five sites (~500 μm apart), 100 nL at each site (~250 μm depth) in the right caudal forelimb area of PV-Cre:Thy1-EGFP mice. Control mice of the same genotype were injected with AAV2/1-CAG-FLEX-tdTomato (UPenn Vector Core). Experimenters were blinded to the identity of the virus before surgeries and each set of experiments contained both opsin and tdTomato animals. Two weeks after the surgery, animals underwent water restriction at 1 mL/d for 14 d. Images of dendritic spines were acquired at the beginning of each behavior session. For ChR2 experiments, blue light pulses from an LED (10-ms pulses, 3 Hz, ~40 mW, 470 nm, Doric Lenses) were delivered directly onto the center of the glass window throughout each behavior session (~30 min). For eNpHR experiments, amber light pulses (10-ms pulses, 10 Hz, ~25 mW, 590 nm, Doric Lenses) were delivered. Control mice received either blue or amber light stimulation in each behavior session and animals were pooled together for analysis. The light power was measured at the tip of the optic fiber (~200 μm in diameter) using a laser power meter.

Two-photon-guided cell-attached recording. ChR2-expressing SOM-IN mice with an imaging window were prepared as above. On the day of the experiment, mice were anesthetized under isoflurane and the glass window was removed. The animals were anesthetized with ketamine (100 mg/kg of body weight) and head-fixed under a two-photon microscope. Loose-patch recordings were performed with glass pipettes (~5–7 MΩ) filled with 200 μM Alexa Fluor 488 in saline. ChR2-tdTomato expressing SOM-INs were identified and targeted for recording. Signals were amplified 100- to 500-fold by the Axon CNS amplifier (Molecular Devices), filtered at 2 kHz, and recorded using Ephus (Matlab) at 10 kHz. In all 15 targeted neurons, blue light stimulation (10-ms pulses, 3 Hz) was applied with alternating blocks of 5 s baseline and 5 s stimulation for up to 20 min. In one of these neurons, after 10 min of this initial recording, blue light stimulation (10-ms pulses, 3 Hz) was applied continuously for additional 10 min.

Statistical analyses. All data points are presented as mean ± s.e.m. except in **Supplementary Figure 5a**, where data points are presented as median. No statistical tests were used to predetermine sample sizes, but our sample sizes are similar to those in previous studies[14,47]. Data in all optogenetics experiments were collected and analyzed blind to the condition of the experiments. In other experiments, only the analyses were performed in blind conditions. Detailed descriptions on the blinding procedure are in the "Image analysis" section. No specific randomization was used for data collection and analyses, but animals were assigned to each experiment without any bias, and both sexes were used in all experiments. Data distribution was assumed to be normal in all experiments, but this was not formally tested. All statistical analyses were performed with Matlab. Statistical significance was determined by bootstrap test, one-way or two-way ANOVA with *post hoc* corrections. Two-tailed tests were used for all comparisons unless indicated.

A **Supplementary Methods Checklist** is available.

40. Li, C.X. & Waters, R.S. Organization of the mouse motor cortex studied by retrograde tracing and intracortical microstimulation (ICMS) mapping. *Can. J. Neurol. Sci.* **18**, 28–38 (1991).
41. Pronichev, I.V. & Lenkov, D.N. Functional mapping of the motor cortex of the white mouse by a microstimulation method. *Neurosci. Behav. Physiol.* **28**, 80–85 (1998).
42. Ayling, O.G., Harrison, T.C., Boyd, J.D., Goroshkov, A. & Murphy, T.H. Automated light-based mapping of motor cortex by photoactivation of channelrhodopsin-2 transgenic mice. *Nat. Methods* **6**, 219–224 (2009).
43. Tennant, K.A. *et al.* The organization of the forelimb representation of the C57BL/6 mouse motor cortex as defined by intracortical microstimulation and cytoarchitecture. *Cereb. Cortex* **21**, 865–876 (2011).
44. Saito, T. & Nakatsuji, N. Efficient gene transfer into the embryonic mouse brain using in vivo electroporation. *Dev. Biol.* **240**, 237–246 (2001).
45. Thévenaz, P., Ruttimann, U.E. & Unser, M. A pyramid approach to subpixel registration based on intensity. *IEEE Trans. Image Process.* **7**, 27–41 (1998).
46. Holtmaat, A. *et al.* Long-term, high-resolution imaging in the mouse neocortex through a chronic cranial window. *Nat. Protoc.* **4**, 1128–1144 (2009).
47. Muñoz-Cuevas, F.J., Athilingam, J., Piscopo, D. & Wilbrecht, L. Cocaine-induced structural plasticity in frontal cortex correlates with conditioned place preference. *Nat. Neurosci.* **16**, 1367–1369 (2013).

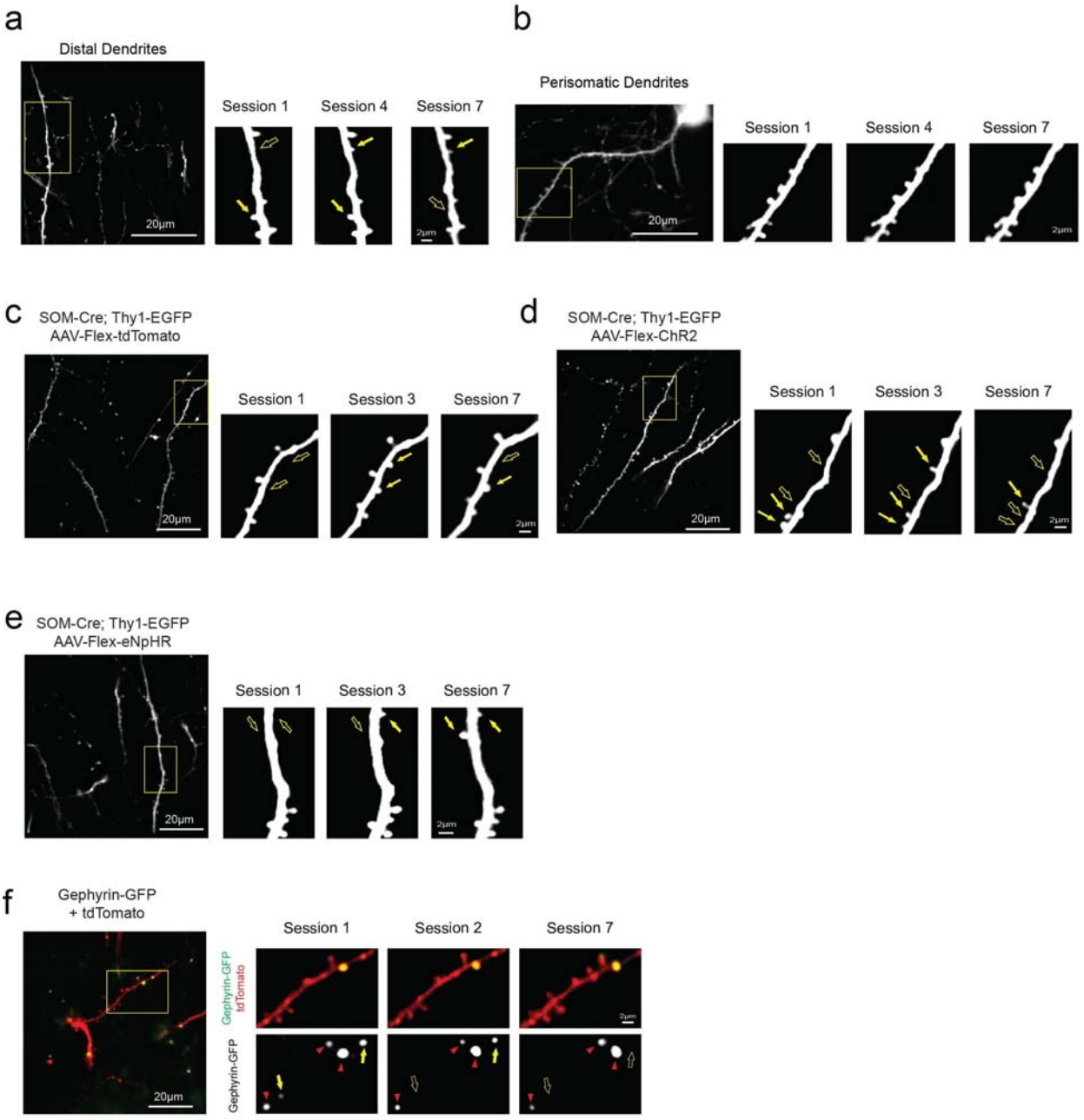

Supplementary Figure 1

Low-magnification images of all representative images.

Low magnification images of the representative images for the L1 distal dendrites of L2/3 excitatory neurons in Fig. 2b **(a)**, the L2/3 perisomatic dendrites of L2/3 excitatory neurons in Fig. 2b (**b**), the L1 distal dendrites in 'Control' in Fig. 7b (**c**), the L1 distal dendrites in 'ChR2' in Fig. 7b (**d**), the L1 distal dendrites in 'eNpHR' in Fig. 7b (**e**), and the L1 distal dendrites in Fig. 6b (red, tdTomato; green, Gephyrin-GFP) (**f**). The smaller panels are the same as those in the main figures.

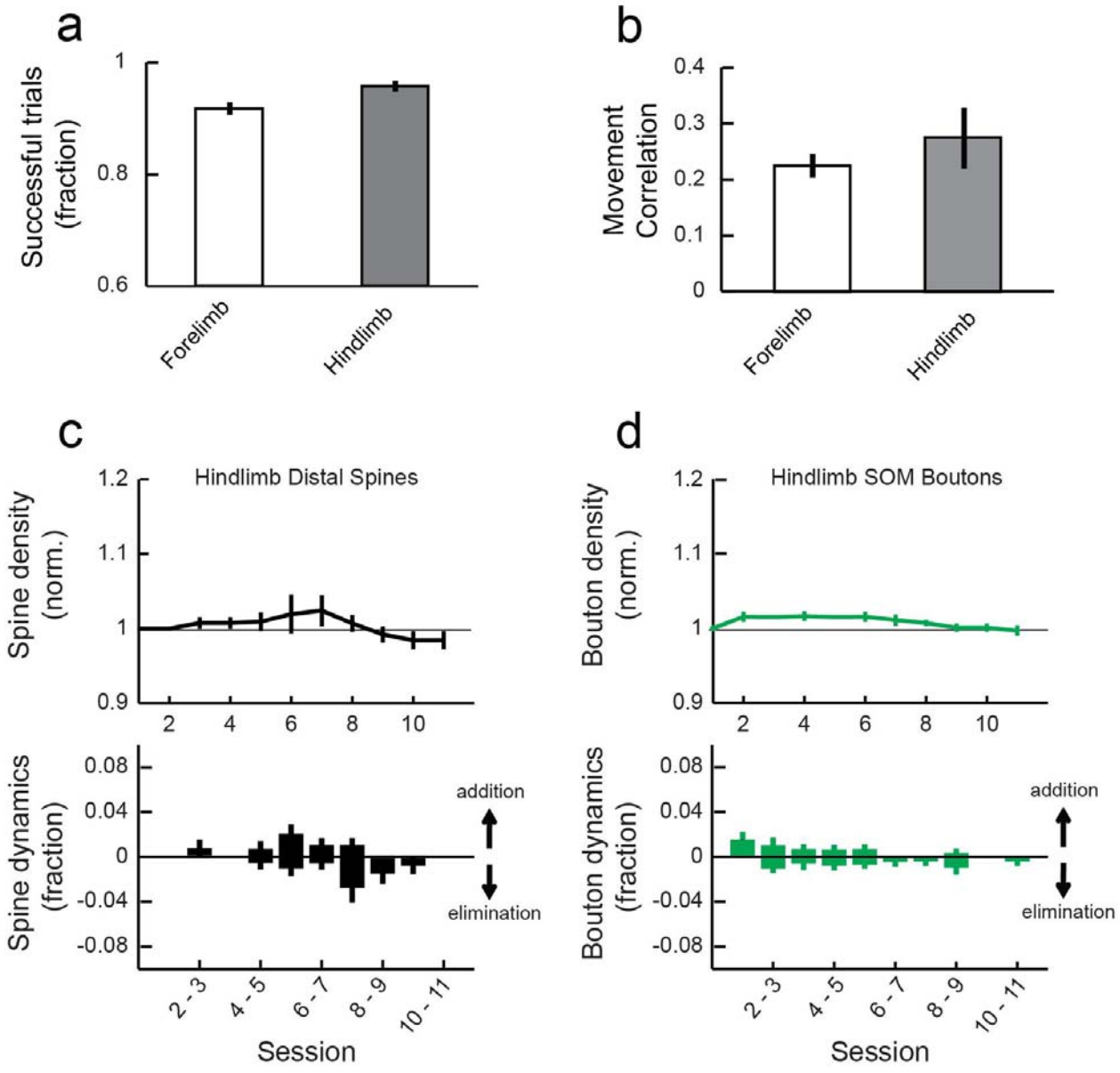

Supplementary Figure 2

Dendritic spines and SOM-IN axonal boutons are stable in the hindlimb area during learning.

(a) Mean fractions of successful trials in sessions 7-11, showing that animals used for hindlimb area imaging learned the task similarly to the animals used for forelimb area imaging. **(b)** Mean of pairwise correlation of rewarded movements in sessions 7-11 in forelimb and hindlimb animals, indicating equivalent levels of learning. **(c)** Mean normalized density (top) and daily dynamics (bottom) of dendritic spines in distal dendrites in the hindlimb area during learning (n = 5 mice, 166 spines). **(d)** Mean normalized axonal bouton density (top) and daily dynamics (bottom) of SOM-INs in the hindlimb area during learning (n = 4 mice, 273 boutons). Both spine and bouton densities are stable during learning and do not show learning-related reorganization (spines, P=0.52; SOM boutons, P=0.07, 1-way ANOVA). Error bars indicate SEM.

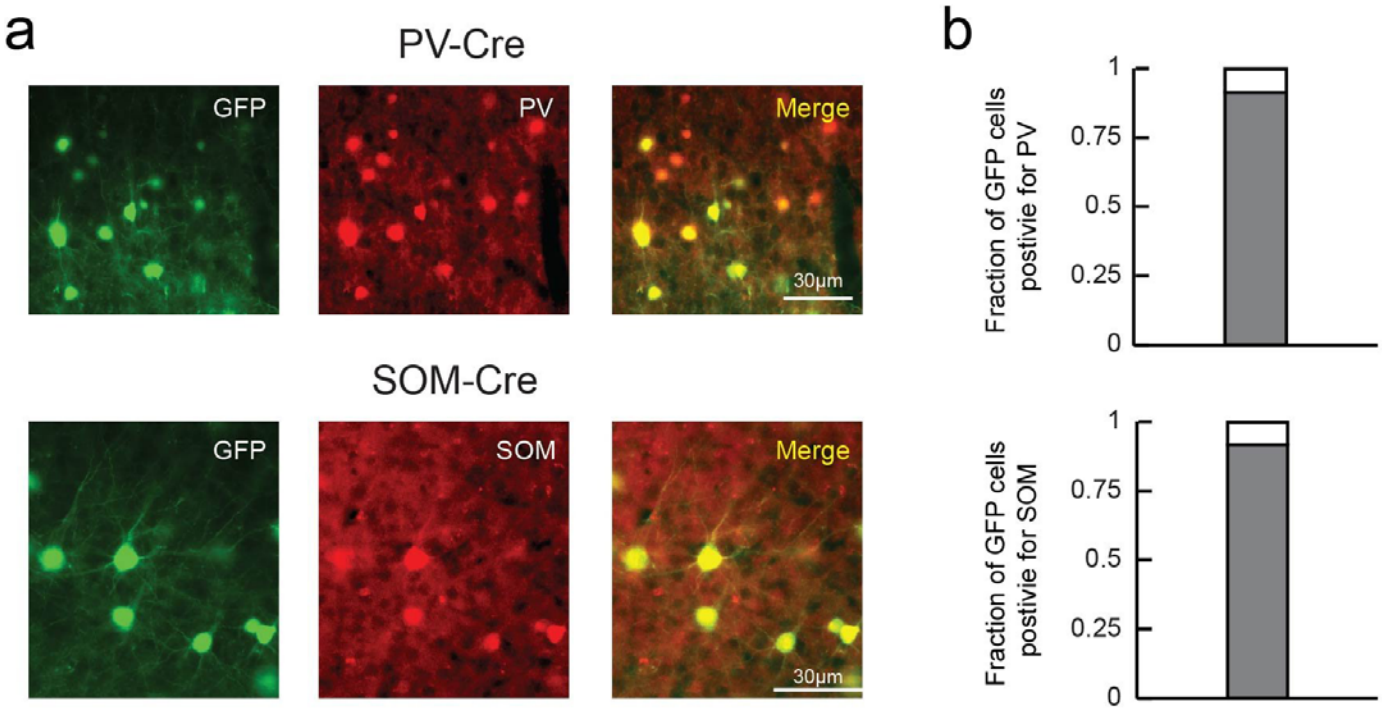

Supplementary Figure 3

Validation of PV- and SOM-IN labeling.

(a) Representative images showing GFP expression in PV or SOM-Cre mouse (left, green) was confined to neurons immunoreactive for PV or SOM (middle, red), respectively. Right panels show merge of two channels. **(b)** Fractions of GFP cells that co-localized with PV (top, 29/32 cells, n = 3 sections from 3 PV-Cre animals) and SOM (bottom, 45/49 cells, n = 3 sections from 3 SOM-Cre animals).

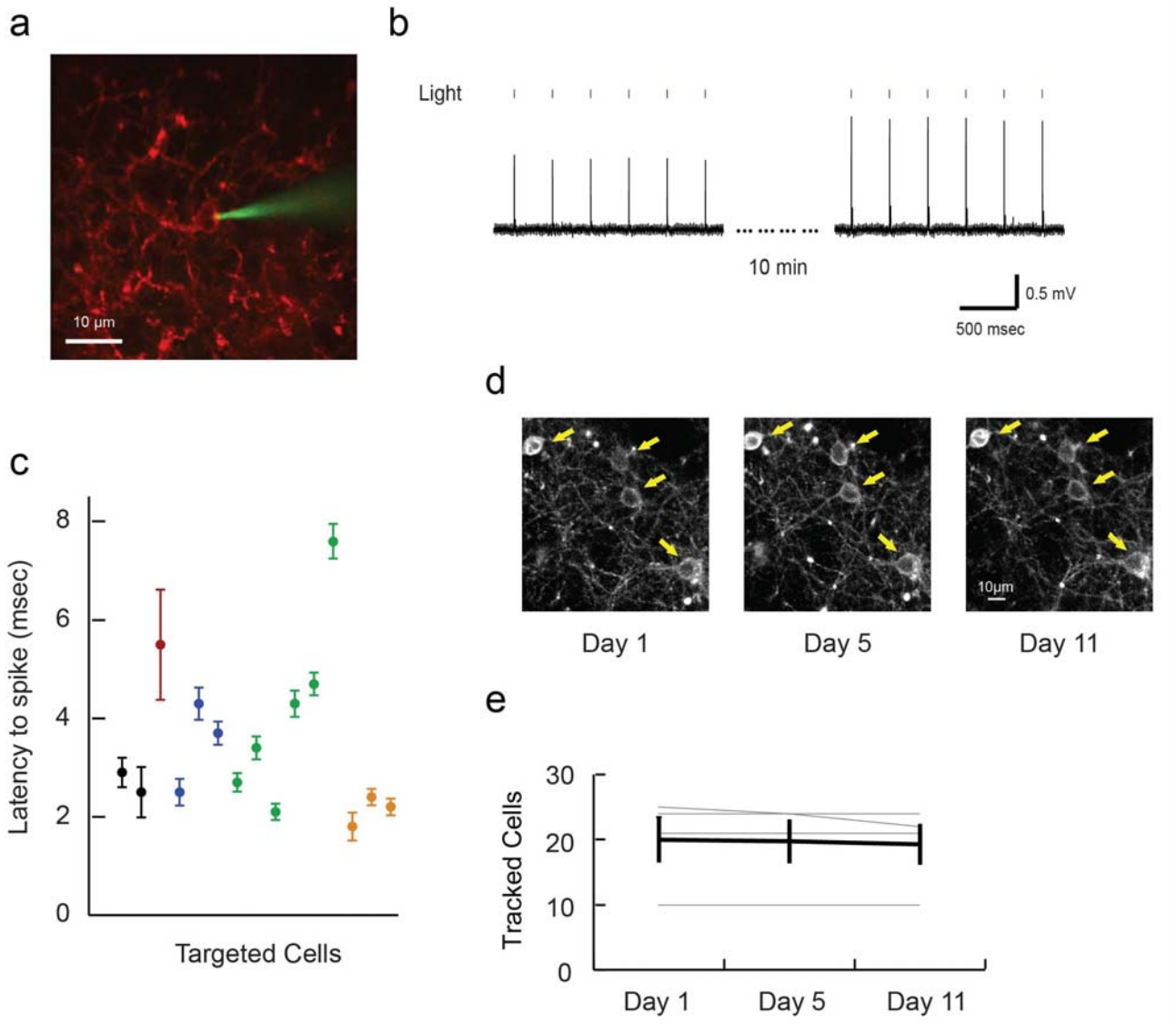

Supplementary Figure 4

Validation of optogenetic stimulation in ChR2-expressing SOM-INs.

(a) Two-photon image of *in vivo* targeted cell-attached recording from a SOM-IN in the motor cortex expressing ChR2-tdTomato (red) and a targeting patch pipette (green). **(b)** Representative traces showing that blue light stimulation (3 Hz, 10 ms/pulse) reliably triggers action potentials in a SOM-IN for the duration of 10 min. **(c)** Latency to spike from light onset (colors represent cells recorded in different animals, n = 15 cells from 5 mice, Median ± SD). **(d)** SOM-INs expressing ChR2-tdTomato were imaged on Days 1, 5, and 11 while blue light stimulation was delivered every day for 11 days (3 Hz, 10 ms/pulse, 30 min/day). Arrows indicate tracked cells. **(e)** Most of SOM-INs were identified throughout the course of the experiment (77/80 neurons remained on Day 11, n = 4 imaging areas in 3 mice), indicating that optogenetic stimulation for 11 sessions does not kill ChR2-expressing SOM-INs. Grey, individual imaging area; black, mean. Error bars indicate SEM.

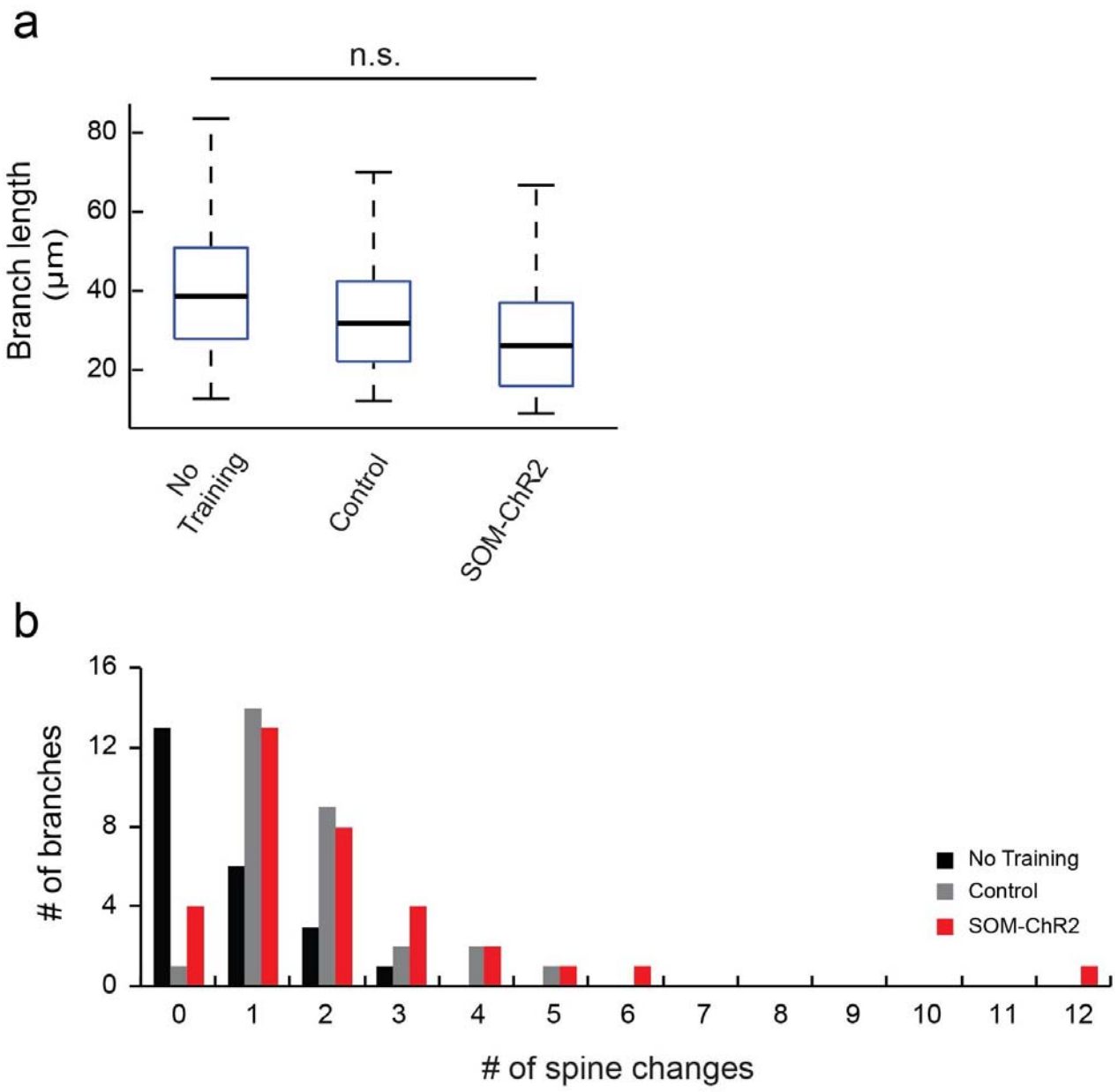

Supplementary Figure 5

Training-induced spine reorganizations are distributed across most branches.

(a) Length of individual dendritic branches analyzed in 'No Training' (n = 23 branches from 5 mice, data from Supplementary Fig. 6), 'Control' (n = 29 branches from 5 mice, data from Fig. 7), and 'ChR2' (n = 35 branches from 5 mice, data from Fig. 7). Branches analyzed in all 3 groups have similar length (P=0.06, 1-way ANOVA). Box plot represents the median (dark line), quartiles (25% - 75% quantiles, white box), and data range (dashed lines). **(b)** Frequency of spine changes on separate dendritic branches. 'Control' and 'ChR2' groups showed more branches with spine changes (P<0.001, chi square test with Bonferroni correction) and more changes within each branch compared to 'No Training' (P<0.01, 1-way ANOVA with post hoc Tukey's test).

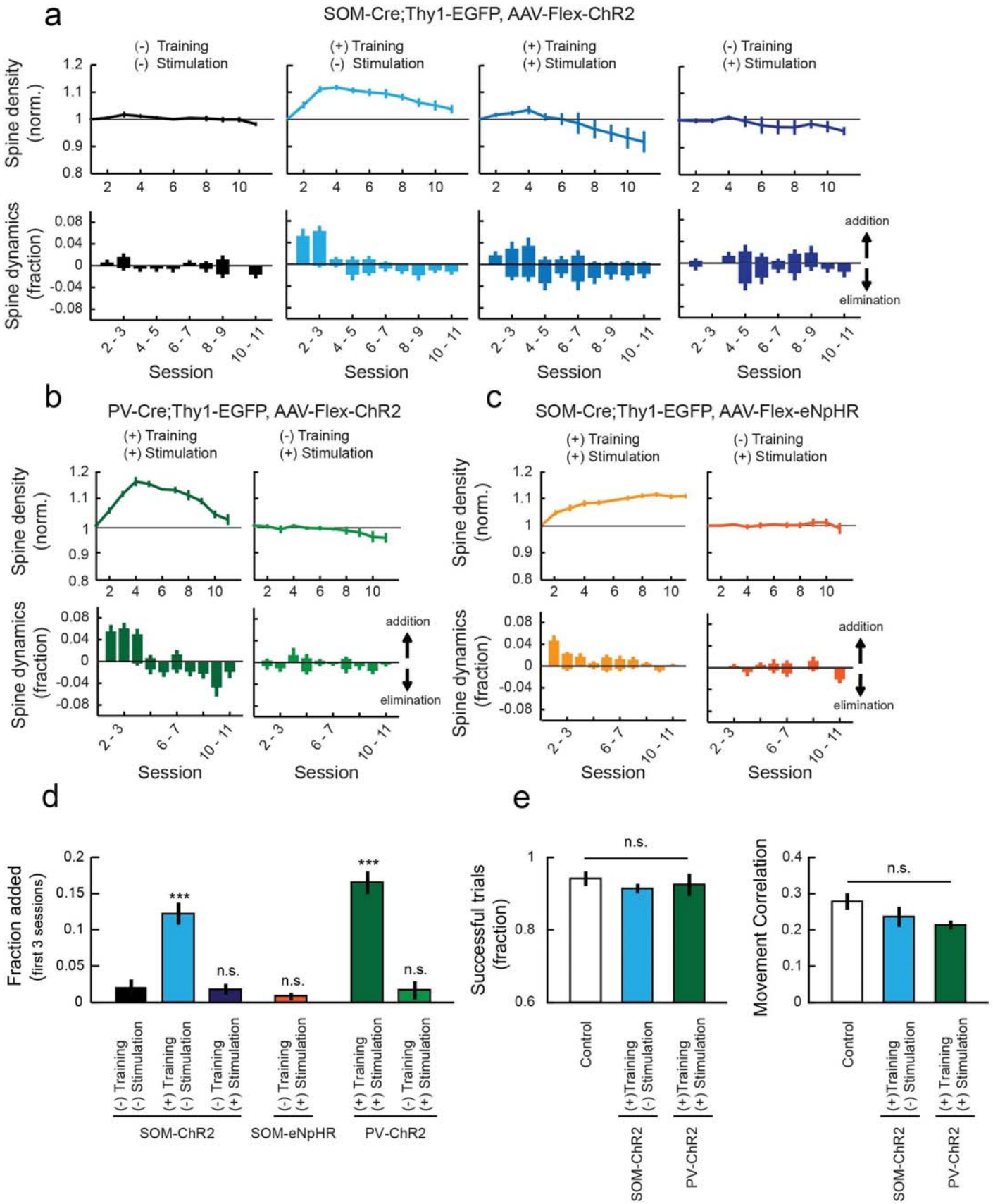

Nature Neuroscience: doi:10.1038/nn.4049

Supplementary Figure 6

Controls for the ChR2 and eNpHR experiments.

(a) Mean normalized spine density (top) and daily dynamics (bottom) of mice expressing ChR2 in SOM-INs. '(-) Training / (-) Stimulation' mice were water restricted and handled but not trained (n = 5 mice, 191 spines). '(+) Training / (-) Stimulation' mice were trained without blue light stimulation (n = 5 mice, 316 spines), '(+) Training / (+) Stimulation' mice received both training and blue light stimulation (n = 5 mice, 255 spines, same data as Fig. 7), and '(-) Training / (+) Stimulation' mice received blue light stimulation without training (n = 5 mice, 180 spines). ChR2 expression alone does not block learning-related spine density increase (P<0.001, '(+) Training / (-) Stimulation', 1-way ANOVA; P<0.001, '(+) Training / (-) Stimulation' vs. '(+) Training / (+) Stimulation'; P=0.19, '(+) Training / (-) Stimulation' vs.'Control, data in Fig. 7', 2-way ANOVA with post hoc Tukey's test). SOM-IN activation alone does not affect spine density (P = 0.24, '(-) Training / (+) Stimulation' vs. '(-) Training / (-) Stimulation', 2-way ANOVA with post hoc Tukey's test). **(b)** Mean normalized spine density (top) and daily dynamics (bottom) of mice expressing ChR2 in PV-INs. '(+) Training / (+) Stimulation', n = 5 mice, 198 spines. '(-) Training / (+) Stimulation', n = 5 mice, 277 spines. Mild activation of PV-INs during learning with the same stimulation protocol as SOM-INs (3 Hz, 10 ms/pulse) does not block learning-related spine density increase (P<0.001, 'PV-ChR2 (+) Training / (+) Stimulation', 1-way ANOVA; P<0.001, 'PV-ChR2 (+) Training / (+) Stimulation' vs. 'SOM-ChR2 (+) Training / (+) Stimulation'; P=0.08, 'PV-ChR2 '(+) Training / (+) Stimulation'' vs. 'Control, data in Fig. 7', 2-way ANOVA with post hoc Tukey's test). **(c)** Mean normalized spine density (top) and daily dynamics (bottom) of mice expressing eNpHR in SOM-INs. '(+) Training / (+) Stimulation', n = 6 mice, 397 spines, same data as Fig. 7. '(-) Training / (+) Stimulation', n = 4 mice, 192 spines. Inactivating SOM-INs without training does not increase spine density (P=0.97, 'SOM-eNpHR (-) Training / (+) Stimulation', 1-way ANOVA; P=0.77, 'SOM-eNpHR (-) Training / (+) Stimulation' vs. 'SOM-ChR2 (-) Training / (-) Stimulation', 2-way ANOVA with post hoc Tukey's test). **(d)** Training consistently induced spine formation in the first 3 sessions in all trained groups. ***P<0.001, 1-way ANOVA with post hoc Tukey's test compared to 'SOM-ChR2 (-) Training / (-) Stimulation'. **(e)** Behavioral performance showing that 'SOM-ChR2 (+) Training / (-) Stimulation' and 'PV-ChR2 (+) Training / (+) Stimulation' animals learned the task, achieving rewards in most trials and developing stereotyped movement. Left, mean fractions of successful trials in sessions 7-11. P=0.63, 1-way ANOVA. Right, mean of pairwise correlation of rewarded movements in sessions 7-11. P=0.14, 1-way ANOVA. The 'Control' group is the same data as in Fig. 8. Error bars indicate SEM.

Experimental Condition	Animal	Spine/Bouton /Puncta	Branch	Branch Length (μm)	Density (/ 100μm)
Apical Dendrites – Forelimb (spine)	1	70	6	147.89	47.33
	2	42	4	83.34	50.40
	3	37	3	76.01	48.68
	4	43	3	101.73	42.27
	5	59	5	117.48	50.22
	Total	**251**	**21**	**526.44**	**47.68**
Basal Dendrites – Forelimb (spine)	1	21	3	43.61	48.16
	2	58	4	114.92	50.47
	3	61	4	126.01	48.41
	4	21	3	42.29	49.66
	5	45	4	69.87	64.40
	Total	**206**	**18**	**396.70**	**51.93**
PV boutons – Forelimb	1	68	4	321.24	36.59
	2	56	4	239.34	38.35
	3	111	9	247.62	37.07
	4	57	6	275.91	34.39
	5	104	8	332.71	31.92
	Total	**433**	**39**	**1416.82**	**30.56**
SOM boutons - Forelimb	1	108	10	185.84	33.62
	2	94	7	146.01	39.27
	3	72	7	299.44	29.08
	4	84	8	165.75	30.44
	5	75	7	325.83	22.54
	Total	**396**	**31**	**1122.86**	**35.27**
Som-Cre:Thy1-EGFP, baseline (spine)	1	31	4	129.37	23.96
	2	41	4	239.07	17.15
	3	48	4	197.19	24.34
	4	38	5	168.12	22.60
	5	33	5	212.09	15.56
	Total	**191**	**22**	**945.84**	**20.19**
SOM-Cre;Thy1-EGFP, Flex-TdTomato, training with stimulation (spine)	1	37	4	125.26	27.14
	2	41	4	123.09	28.43
	3	55	8	266.96	20.60
	4	39	6	158.03	24.68
	5	50	8	222.20	22.50
	6	22	3	98.31	22.38
	7	53	8	164.85	32.15
	8	72	4	263.90	27.28
	9	86	9	205.33	41.88
	10	67	8	359.21	18.65
	11	68	9	183.08	37.14
	12	75	11	209.88	35.73
	Total	**665**	**82**	**2380.08**	**27.94**
Distal Spine - Forelimb Baseline	1	65	7	245.66	26.46
	2	47	5	115.87	40.56
	3	52	6	133.15	39.05
	4	21	1	63.46	33.09
	5	19	2	86.48	21.97
	6	33	2	89.93	36.69
	7	20	3	104.50	19.13
	Total	**257**	**26**	**839.05**	**30.99**
Perisomatic Spine - Forelimb Baseline	1	34	4	129.41	26.27
	2	21	3	108.11	19.42
	3	36	5	108.17	33.28
	4	22	2	107.03	20.55
	Total	**113**	**14**	**452.72**	**24.88**
SOM boutons - Forelimb Baseline	1	83	9	345.39	24.03
	2	61	9	232.06	26.29
	3	63	6	154.30	40.83
	4	86	4	251.85	34.15
	5	81	4	240.09	33.74
	6	90	6	392.30	22.94
	Total	**464**	**38**	**1615.99**	**28.71**
PV boutons - Forelimb Baseline	1	85	7	205.12	41.44
	2	139	12	469.61	29.60
	3	89	8	246.93	36.04
	4	52	6	209.43	24.83
	5	65	4	210.52	30.88
	6	58	5	251.16	23.09
	Total	**488**	**42**	**1592.77**	**30.64**
Apical Dendrites – Hindlimb (spine)	1	35	3	164.23	21.31
	2	36	4	206.80	17.41
	3	28	4	131.43	21.30
	4	26	3	145.78	17.84
	5	41	3	153.39	26.73
	Total	**166**	**17**	**801.62**	**20.71**
SOM boutons – Hindlimb (spine)	1	56	3	210.53	26.60
	2	85	6	221.94	38.30
	3	68	4	233.16	29.16
	4	64	6	207.29	30.87
	Total	**273**	**19**	**872.91**	**31.27**

Experimental Condition	Animal	Spine/Bouton/ Puncta	Branch	Branch Length (μm)	Density (/ 100μm)
SOM-Cre;Thy1-EGFP, Flex-ChR2, training with stimulation (spine)	1	28	4	146.24	19.15
	2	67	10	298.31	22.46
	3	61	10	190.45	32.03
	4	74	9	278.84	26.54
	5	25	5	124.89	20.02
	Total	**255**	**38**	**1038.73**	**24.55**
SOM-Cre;Thy1-EGFP, Flex-ChR2, no training with stimulation (spine)	1	32	4	112.40	28.47
	2	45	4	135.70	33.16
	3	29	5	128.71	22.53
	4	31	5	150.95	20.54
	5	43	5	146.16	29.42
	Total	**180**	**23**	**673.93**	**26.71**
SOM-Cre;Thy1-EGFP, Flex-ChR2, training with no stimulation (spine)	1	57	6	232.29	24.54
	2	89	8	293.46	30.33
	3	35	3	143.78	24.34
	4	72	7	278.03	25.90
	5	63	7	157.61	39.97
	Total	**316**	**31**	**1105.18**	**28.59**
SOM-Cre;Thy1-EGFP, Flex-eNpHR, training with stimulation (spine)	1	61	7	190.20	32.07
	2	82	7	320.30	25.60
	3	68	13	186.60	36.44
	4	53	9	178.50	29.69
	5	64	8	387.61	16.51
	6	69	8	332.73	20.74
	Total	**397**	**52**	**1595.94**	**24.88**
SOM-Cre;Thy1-EGFP, Flex-eNpHR, no training with stimulation (spine)	1	32	4	139.56	22.93
	2	37	6	141.59	26.13
	3	51	4	184.64	27.62
	4	72	5	233.46	30.84
		192	**19**	**699.25**	**27.46**
PV-Cre;Thy1-EGFP, Flex-ChR2, training with stimulation (spine)	1	40	3	185.23	21.59
	2	28	3	79.88	35.05
	3	44	7	159.74	27.54
	4	58	7	186.14	31.16
	5	28	3	112.66	24.85
	Total	**198**	**23**	**723.66**	**27.36**
PV-Cre;Thy1-EGFP, Flex-ChR2, no training with stimulation (spine)	1	65	6	249.27	26.08
	2	73	7	287.50	25.39
	3	52	7	164.22	31.66
	4	57	6	140.95	40.44
	5	30	5	141.80	21.16
	Total	**277**	**31**	**983.73**	**28.16**
Gephyrin puncta – Baseline	1	42	10	240.64	17.45
	2	33	6	206.14	16.01
	3	63	8	324.88	19.39
		138	**24**	**771.66**	**17.88**
Gephyrin puncta - Training	1	54	9	458.30	11.78
	2	95	11	458.91	20.70
	3	80	10	408.90	19.56
	4	110	14	771.74	14.25
	Total	**339**	**44**	**2097.85**	**16.16**

Total Animals	**107**
Total Spine/Bouton/Puncta Scored	**6082**
Total Branch Covered (mm)	**23.82**

Supplementary Table 1
Summary of number of mice, spines/boutons/puncta, branch number, branch length, and density in all experimental conditions

Nature Neuroscience: doi:10.1038/nn.4049